A newly distinguished marine magnetotelluric coast effect sensitive to the lithosphere-asthenosphere boundary

Shunguo Wang[1], Steven Constable[1], Valeria Reyes-Ortega[1], Catherine A. Rychert[2]

[1]*Scripps Institution of Oceanography, University of California San Diego, La Jolla, California, USA.*

[2]*Ocean and Earth Science, University of Southampton, Southampton, UK.*

Corresponding author: Shunguo Wang, s4wang@ucsd.edu, +1(858)3449026

SUMMARY

The marine magnetotelluric (MT) method is a useful tool for offshore studies aimed at, for example, hydrocarbon exploration and the understanding of Earth's tectonics. Marine MT data are often distorted by coastlines because of the strong resistivity contrast between the conductive ocean and the resistive land. At mid ocean ridges, the resistivity of Earth's structure can be assumed to be two-dimensional (2D), which allows MT data to be decomposed into a transverse electrical (TE) mode, with electric current flowing approximately along the ridge, and a transverse magnetic (TM) mode, with electric current flowing perpendicular to the ridge. We collected marine MT data at the middle Atlantic Ridge which exhibited highly negative TM-mode phases, as large as -180°, at relatively high frequencies (0.1 to 0.01 Hz). Similar negative phases have been observed in other marine MT datasets, but have not been the subject of study. We show here that these negative phases are caused by a newly distinguished coast effect. The TM-mode coast effect is not only a galvanic effect, as previously understood, but also includes inductive distortions. TM-

mode negative phases are caused by the turning of the Poynting vector, the phase change of electromagnetic fields, and vertically flowing currents in the sea floor. The findings provide a new understanding of the TM-mode coast effect, which can guide our ability to fit the field data with the inclusion of coastlines, and reduce misinterpretation of the data in offshore studies. The study also shows that the TM-mode coast effect is sensitive to the depth and conductivity of the asthenosphere, an important feature of the Earth's interior that was the object of our Atlantic Ocean study.

Key words: Marine electromagnetics; Magnetotellurics; Electromagnetic theory; Mid-ocean ridge processes; Electrical properties

1 INTRODUCTION

The marine magnetotelluric (MT) method, using natural-source signals, plays an important role in our understanding of Earth's interior at mid-ocean ridges (e.g. Key *et al.* 2013), hotspots (e.g. Nolasco *et al.* 1998), oceanic trenches and subduction zones (e.g. Naif *et al.* 2013; Worzewski *et al.* 2011), especially for situations relating to melting and de-/hydration. In 2017, we deployed 39 marine MT instruments across the Middle Atlantic Ridge (MAR), 500 – 1500 km away from the African coast (Fig. 1a), to study the evolution of the lithosphere-asthenosphere boundary (LAB) with age. The instruments were deployed for a year alongside an array of ocean-bottom seismometers as part of the Passive Imaging of the Lithosphere-Asthenosphere Boundary (PI-LAB) experiment (Agius *et al.* 2018; Harmon *et al.* 2018), but acquisition time was limited to 60 days by the MT instrument battery life. However, the time series was long enough to process data to a low frequency of 5×10^{-5} Hz. Two examples of MT response functions, at stations 11 and 15 along one profile, are shown in Figs 1(b) - (e). A striking feature of these data is negative phases

between 0.1 and 1×10^{-2} Hz (Figs 1c and e) in the mode in which the electric field is approximately perpendicular to the ridge (the transverse magnetic mode as described below). This effect was seen in most of the stations at the eastern side of MAR along the profiles. We initially assumed that this was caused by an instrument calibration issue or a processing error, but we have eliminated these possibilities by carefully checking the instruments and algorithms used. Since negative phases are non-causal for one-dimensional (1D) structure, this effect has to be caused by two-dimensional (2D) or three-dimensional (3D) structures.

In 2D survey geometries, MT data can be decomposed as two independent modes, transverse electric (TE) and transverse magnetic (TM), based on different polarization directions of the MT signals. Phase anomalies, larger than 90° or negative, have been observed in land/coastal MT data (e.g. Pek & Verner 1997; Heise & Pous 2003; Lezaeta & Haak 2003; Weckmann *et al.* 2003; Ichihara & Mogi 2009). A L-shaped conductor model and the physics of current channeling combined with 2D anisotropic or 3D isotropic models were used to explain these phase anomalies (e.g. Lezaeta & Haak 2003; Ichihara & Mogi 2009). These studies show the importance of understanding the physics of phase anomalies in land/coastal MT data, since it would be difficult for inversion algorithms to find these kinds of models without guidance. However, these explanations do not represent what we have observed in our dataset, since our observations are far away from any continents, and severe current channeling is difficult in the presence of uniformly conductive seawater. We attempted 2D anisotropic inversions and were not able to fit the field data. We need to seek another explanation for the highly negative phases we observed at the MAR.

Marine MT TE and TM-mode data are distorted differently by the coast. TE-mode data, in which electric currents flow parallel to structure, suffer from inductive distortion shown as upward cusps in the apparent resistivities and negative phases (Constable *et al.* 2009; Key & Constable

2011; Worzewski *et al.* 2012). The physics behind the TE-mode distortion, especially for the negative phases, was shown to be inductive currents flowing along the edge of the deep ocean basin, with electromagnetic energy diffusing down through the onshore section and bending laterally and then back upwards to the seafloor (Key & Constable 2011). This effect was also observed in land MT data when data were collected near large resistivity contrasts (Selway *et al.* 2012). Our previous understanding of the TM-mode coast effect distortion, in which electric currents flow perpendicular to structure, is that it is a galvanic distortion associated with electric currents flowing in seawater being deflected by the resistive land, which leads to depressed apparent resistivities. Because the distortion is galvanic, phases are largely unaltered, and the influence can propagate to large distances, particularly at low frequencies (Bailey 1977; Cox 1980; Ranganayaki & Madden 1980; Menvielle *et al.* 1982; Monteiro Santos *et al.* 2001; Alekseev *et al.* 2009; Constable *et al.* 2009; Key & Constable 2011; Worzewski *et al.* 2012). This model of the TM-mode coast effect does not explain the prominently negative phases observed in our MAR dataset at the high frequencies. A similar phenomenon was observed in data collected offshore of northeastern Japan (Key & Constable 2011), but the 2D inversion of that dataset did not fit this distorted part of the data, and the authors did not investigate the physics behind this feature. Later, in an offshore Costa Rica study (Worzewski *et al.* 2012), negative TM phases were observed but not studied.

Before we quantitatively model our MT data from the MAR, which likely will require 3D inversions to fully capture the geometry of the coast and seafloor structure, we seek to understand the physics of the TM-mode negative phases. As we explain above, it is likely that our inversions will need to be guided by our understanding of the physics. At this time, no publicly available 3D code can handle the bathymetry and distant coastlines required by our dataset. We therefor use 2D

92 modeling due to its availability and efficiency, and the TE and TM-mode physics can separate in
93 2D models. The physics is similar in 3D structure, but intermingled. In this study, TM-mode data
94 are modeled with simple 2D ocean models, and the physics behind the TM-mode negative phases
95 is examined using the Poynting vector, electromagnetic (EM) fields, and electric current density.
96 We also investigate the influence of model parameters of seawater depth and oceanic lithosphere
97 and asthenosphere on the TM-mode coast effect.

98

99 **2 METHODS**

100 In the frequency domain, the observed MT electric fields (E_x, E_y) and MT magnetic fields (H_x, H_y)
101 are related through the frequency-dependent impedance tensor $\boldsymbol{Z}$ given as

102 $$\begin{bmatrix} E_x \\ E_y \end{bmatrix} = \begin{bmatrix} Z_{xx} & Z_{xy} \\ Z_{yx} & Z_{yy} \end{bmatrix} \begin{bmatrix} H_x \\ H_y \end{bmatrix}, \quad (1)$$

103 where a Cartesian coordinate system is used in which x represents strike direction, y profile
104 direction, and z positive downwards.

105 In 2D media, the diagonal components of $\boldsymbol{Z}$ are zero, and the off-diagonal components Z_{xy}
106 and Z_{yx} can be used to define apparent resistivities ($\rho_{xy/yx}$) and phases ($\phi_{xy/yx}$) of TE and TM-
107 mode, respectively, as

108 $$\rho_{xy/yx} = \frac{1}{\mu\omega}\left|Z_{xy/yx}\right|^2, \quad (2)$$

109 $$\phi_{xy/yx} = \tan^{-1}\left(\mathrm{Im}\left(Z_{xy/yx}\right)/\mathrm{Re}\left(Z_{xy/yx}\right)\right), \quad (3)$$

110 where μ is permeability, and ω is angular frequency.

111 The EM energy diffusion and propagation path can be illustrated using the complex
112 Poynting vector (Stratton 2015):

113 $$\boldsymbol{S} = \frac{1}{2} Re(\boldsymbol{E} \times \boldsymbol{H}^*), \quad (4)$$

114 where $\boldsymbol{H}^*$ represents the conjugate of magnetic field $\boldsymbol{H}$, and $\boldsymbol{E}$ represents electric field. For the
115 TM-mode case, Equation 4 can be simplified as

116 $$\boldsymbol{S} = \frac{1}{2} Re(E_z \cdot H_x^* \hat{\boldsymbol{y}} + E_y \cdot H_x^* \hat{\boldsymbol{z}}), \quad (5)$$

117 $\hat{\boldsymbol{y}}$ and $\hat{\boldsymbol{z}}$ represent the unit vector in the y and z directions. The electric fields E_y and E_z and the
118 magnetic field H_x have non-zero values when TM-mode fields are considered. The tool used to
119 calculate EM fields is MARE2DEM (Key 2016) which is a well-tested academic code.

120 The current density in the yz-plane is given by

121 $$\boldsymbol{J} = (\sigma - \mathrm{i}\varepsilon\omega) \cdot (E_y \hat{\boldsymbol{y}} + E_z \hat{\boldsymbol{z}}), \quad (6)$$

122 where σ is the conductivity, inverse of resistivity, of media, i represents imaginary unit, and ε is
123 permittivity of media. Displacement current density given by the $\mathrm{i}\varepsilon\omega$ term is negligible in our case
124 because ocean and seafloor conductivities are relatively high and frequencies relatively low. The
125 real part of the current density can illustrate the physical quantities (Boas 2006). This approach
126 may potentially neglect some of the physics (Raziman & Martin 2016), but, current flows will be
127 hard to illustrate without using it (Pek & Verner 1997), and it is similar to using real components
128 of tipper as induction arrows and using real component of electric fields as directional arrows
129 (Parkinson & Jones 1979; Ichihara & Mogi 2009).

130

3 RESULTS

3.1 Induction coast effect in TM-mode data

We use a simple ocean model to model the coast effect in TM-mode data and to understand its physics (Fig. 2). Bathymetry is not considered in the model in order to make the results easier to understand. The depth and resistivity of an ocean are 5 km and 0.33 Ωm, respectively. The coast is at the 2500 km position along the profile in the *y* direction. The thickness and resistivity of the seafloor/lithosphere are chosen as 45 km and 10,000 Ωm, respectively. The resistivity of the asthenosphere is 10 Ωm.

The high resistivity of the oceanic lithosphere is a critical parameter in the propagation of the TM-mode coast effect (Heinson & Constable 1992). Once controversial, it is now widely known, mainly from deep marine controlled source EM sounding data (e.g. Constable & Cox 1996) but also MT data sensitive to the coast effect (Mackie *et al.* 1988), that the dry and cool oceanic upper mantle has a resistivity of about 10,000 Ωm.

We find that the observed negative phases implies that the coast effect in TM-mode data is not only a galvanic but also an inductive phenomenon, as speculated by Worzewski et al. (2012). The TM-mode apparent resistivities and phases at frequencies of 1.0×10^{-4} and 5.0×10^{-2} Hz based on the simple ocean model are shown in Fig. 2 (a large range of frequencies were tested from 1.0×10^{-1} to 1.0×10^{-5} Hz, the results of other frequencies are shown in the supplementary Video I). Even though the difference in apparent resistivities between Figs 2(a) and (b) is not prominent for the coast effect at distances of 1500 to 2500 km, the differences in phases between Figs 2(c) and (d) show that the TM-mode coast effect is frequency-dependent.

152 The frequency-dependence feature is more obvious when the apparent resistivities and
153 phases of thirteen frequencies are compared (Fig. 3). TM-mode apparent resistivities are more
154 strongly depressed than TE-mode ones (Figs 3a and b). TE negative phases exist mainly at the
155 positions close to the coastline (Fig. 3c), and TM-mode negative phases exist, however, at a
156 surprisingly large distance, as much as 800 km (Fig. 3d). Thus, the TM-mode coast effect at low
157 frequencies is expressed mainly as depressed apparent resistivities, but is expressed as depressed
158 apparent resistivities and negative phases at relatively high frequencies (Figs 2 and 3).

159 Noticeably, the TM-mode negative phases and relatively high apparent resistivities at high
160 frequencies (Figs 3e and f) are able to approximately represent the phenomenon we observed in
161 our field data (Figs 1b - d). The reason we cannot accurately model the field data is that both the
162 coastline and bathymetry have some 3D effects we cannot fully capture in the 2D modeling.

163

164 **3.2 Physics behind TM-mode negative phases**

165 The turning of the Poynting vector direction, originated from the top of the model and
166 shown as bending white streamlines in Figs 2 and 4, is related to the TM-mode negative phases.
167 The H_x field is enhanced in the seafloor near to the coast due to induction (Fig. 4a) compared to
168 the fields far away from the coast. The E_y field is deflected due to the coast (Fig. 4b), which causes
169 the feature of depressed apparent resistivity. The E_z field is, however, enhanced near the coast due
170 to the current flowing downwards even when compared to the E_y field (Figs. 4b and c). Thus, the
171 path of EM energy propagation represented by the Poynting vector starts to have strong horizontal
172 component (governed by H_x and E_z fields in Equation 5) near to the coast and bends from the coast
173 to the ocean (Figs 2 and 4). The direction of the Poynting vector becomes parallel to the ocean

bottom when the E_y field is negligible (Fig. 4b, Equation 5). Then the Poynting vector starts to finish a 'U' turn and propagate upwards. Thus, back propagation of EM energy, indicated by the turning of the Poynting vector, is related to the TM-mode negative phase. The phases of the H_x and E_z fields in Figs 4(d) and (f) also indicate the direction change of the fields (Fig. 4d shows the phase of $-H_x$). The phase reversal of TM-mode data is related to the phase changes of the H_x and E_y fields (Figs 4d and e). This is a similar phenomenon to the phase reversal observed in TE-mode data, which is related to the phase reversal of H_y field.

Extracting the real component of the complex-valued current density to obtain physical information may potentially lead to a pitfall based on a recent study (Raziman & Martin 2016). However, this is a way to illustrate the currents when they are complex-valued and have two spatial components (e.g. Pek & Verner 1997; Ichihara & Mogi 2009). Thus, current flows represented by the real component of current density also provide useful information to understand the physics of the TM-mode coast effect. The strong contrast of resistivity at the coast depletes the currents, C1 and C2 in Fig. 5(a), in the *y* direction and causes the current, C3 in Fig. 5(a), to flow downwards, even though the current, C2 in Fig. 5(a), from land may flow upwards due to sea water attraction. The upward current, C4 in Fig. 5(a), is partially induced by the decreasing magnetic field (Figs 4a and 5a). Its direction opposes the current, C3 in Fig. 5(a), propagating downwards. The displacement current (Fig. 5b) is negligible compared to the conduction one (Fig. 5a).

In order to illustrate current flows in a clear way, a sketch of current flows is useful (Fig. 6). No vertical current is generated when current, such as the current C1, flows horizontally without the distortion of the coast (Fig. 6a). When the coast exists, currents both from ocean (the current C1) and land (the current C2) merge together at the coast and then flow downwards as the current C3 (Fig. 6b). Since different amount of charges are accumulated at the boundaries of the

lithosphere, this can lead to a voltage difference. For example, voltage V2 at the bottom of the lithosphere is higher than voltage V1 at the top of the lithosphere, this can be confirmed in Figs 4(b) and (c) at the distances, for example, of 2,000 to 2,500 km at the 20 km depth to shallower depths, especially in Fig. 4(b). Also, based on Lenz's law, when the magnetic field is decreasing, an induced current should create a magnetic field which has the same direction as the decreasing one. The current C4 is able to play such a role here (illustrated in Fig. 5a). It seems these currents form a loop, which interestingly fits the explanation of coast effect in Parkinson & Jones (1979). Thus, probably due to the voltage difference and induction of magnetic field, the current flows upwards (Fig. 6b). At relatively high frequencies, the H_x field which propagates from the sea surface to the seafloor is attenuated by the conductive ocean (Constable 2013). This allows the induced H_x field (marked as red color, Fig. 6b) to dominate in the seafloor/lithosphere and also explains why the TM-mode negative phases existed at relatively high frequencies. Based on the analyses, TM-mode phases can get reversed due to the phase change of E_y and phase change of induced H_x compared to the original fields in the ocean, as shown in Fig. 6(b).

To conclude, TM-mode coast effect shown as phase reversal and depressed apparent resistivity at relatively high frequencies (Figs 2b and d) is caused by the diffusion and back propagation of EM energy, phase change of E_y and H_x fields due to depression and induction respectively, downward current due to depression, and upward current probably due to induction and voltage difference, evident where the original H_x field is attenuated in the seawater. This high-frequency TM-mode coast effect is more complicated than the low frequency TM-mode coast effect, which is exhibited mainly as depressed apparent resistivities and has been previously well studied (e.g. Bailey 1977; Cox 1980; Ranganayaki & Madden 1980; Menvielle *et al.* 1982; Monteiro Santos *et al.* 2001; Alekseev *et al.* 2009; Constable *et al.* 2009). This understanding

should help us interpret our field data using the available modeling tools, while a marine MT 3D inversion code with a capacity to model distant coastlines and bathymetry is developed.

3.3 Influence of the asthenosphere on the coast effect

Various models with different parameters are used to show the sensitivity of the TM-mode coast effect to the LAB. The TM-mode coast effect is sensitive to the conductive layer, representing the asthenosphere layer, that lies beneath the seafloor (Figs 7 and 8). It seems the existence of the asthenosphere layer allows more current to flow down near the coast zone (Figs 7a, 7c, 8a and 8c). The TM-mode inductive coast effect, caused by the phase changes of H_x and E_y fields due to the depression of the E_y field, can show up at a large propagation distance. The TM-mode coast effect becomes stronger in Fig. 7(a) than in Fig. 7(c) at the depths larger than 50 km, since the signals have a larger penetration depth when no conductive layer lies beneath the seafloor. Generally, the negative phase of the TM-mode coast effect can be more pronounced when one of these conditions is satisfied: (1) an asthenospheric conductor exists (Figs 7a and c); (2) the resistivity contrast between lithosphere and asthenosphere is larger (Figs 7c-e, 8c-d); (3) lithospheric thickness is larger (Figs 7e-f, 8e-f); and (4) the ocean depth is larger (Figs 7b-c). However, it can be less pronounced when the product of the resistivity and thickness of the seafloor (the transverse resistance) is increased (Figs 7d and f). Whether and where negative phases show up depends on the frequency, the existence of asthenosphere, the resistivity contrast of the lithosphere and asthenosphere, the lithosphere thickness, and the ocean depth. The existence of negative phases indicates inductive distortion, but the position where they occur is related to both inductive and galvanic distortions.

The distance to the coast where back propagation of EM energy reaches a maximum can be approximated with the strategy proposed by Cox (1980), which is $L = \sqrt{h_o h_l \rho_l / \rho_o}$ m away from coastlines (the resistivity of the ocean, ρ_o, is often taken as 0.33 Ωm). However, the furthest distance corelated to the negative phases is only around half of *L*. The low current density under the seafloor is related to the reversal of current directions (Fig. 8). Upward flowing currents are partially corelated to the induced magnetic field as shown in Figs 5(a) and 6(b). The result indicates that marine MT data are sensitive to the LAB, and proper interpretation of marine MT data must consider the coast effect, which plays an important role here.

3.4 Potential problems caused by the coast effect

The TM-mode coast effect described here affected the study of Key & Constable (2011) offshore northeastern Japan, as two stations showed a bad data fit for TM-mode phases at high frequencies, (stations s04 and s01 in Fig. 3 of Key & Constable, 2011). Now this coast effect has been identified in our study, future inversions of these, and other, datasets can be guided to fit distorted data, which is otherwise difficult to fit using unconstrained 2D isotropic and anisotropic inversions. Synthetic tests also revealed that it was hard to resolve the real shape of the anomaly in a synthetic model. The main reason this effect has only recently come to our attention is that the early marine MT datasets were collected at relatively low frequencies where this effect is not visible. Using the method of subtracting coast effect proposed by Dosso & Meng (1992) or using the determinant of the impedance tenser for inversion proposed by Pedersen & Engels (2005) to

suppress 3D effect might potentially mitigate the influence or part of it, but this will be the subject of another study.

4 DISCUSSION AND CONCLUSIONS

Like the TE-mode coast effect, the TM-mode effect is frequency-dependent, which is different from what previous studies have assumed. At low frequencies, the TM-mode coast effect shows as depressed apparent resistivities and unaltered phase. At high frequencies at sufficient distance from the coast it shows, however, as depressed apparent resistivities and negative phases. TM-mode negative phases are an obvious feature of inductive distortion. Thus, the coast effect in marine MT TM-mode data is a combination of galvanic and inductive distortions. The TM-mode coast effect exhibits as phase reversal and depressed apparent resistivity at relatively high frequencies caused by the diffusion and back propagation of EM energy, phase change of EM fields due to depression and induction, downward current due to depression, and upward current probably due to induction and voltage difference. The negative phases of TM-mode data exist when the original magnetic source field is attenuated in the ocean, and an induced magnetic field dominates in the lithosphere. Even though we focused on the TM-mode coast effect in marine MT data, the TM-mode coast effect in land MT data and the TE-mode coast effect both in marine and land MT data are shown in the supplementary Video I.

A conductive asthenosphere beneath the seafloor can enhance the TM-mode coast effect, since the vertical currents caused by the coast can flow more easily as the conductive layer attracts the current. Furthermore, the TM-mode coast effect is sensitive to the resistivity contrast of the seafloor/lithosphere and the underlying asthenosphere, the lithosphere thickness, and the ocean

depth. These indicate that the relatively long period MT data we collected at MAR are sensitive to the LAB, whose depth is still an elusive topic. Thin sheet models often used to model the coastlines and seafloor bathymetry will not work well for the removal of the TM-mode coast effect at relatively high frequencies, since the method is only accurate for long period MT data (Price 1949; Ranganayaki & Madden 1980).

One should note that the coast effect described by our 2D modeling may not fully explain 3D effects in the data, even though the physics is similar and intermingled. We have not yet exactly modeled the coast effect in our field data due to the complicated geometry of coastline and bathymetry. Quantitative interpretation of our data is likely to require a fully inductive 3D model that can accommodate the shape of the coastlines as well as the local MAR geology, which is currently a challenging, perhaps even unsolved, computational problem.

ACKNOWLEGMENTS

This research was supported by National Science Foundation under grant OCE-1536400. We thank the captains and crews of the R.V. Marcus G. Langseth and the R.R.S. Discovery for support with the deployments and recoveries, and N. Harmon acting as one of the Chief Scientists on the deployment and recovery cruises. Data and field log are available on http://marineemlab.ucsd.edu. S. Wang thanks the Green Foundation at the Institute for Geophysics and Planetary Physics and the Seafloor Electromagnetic Methods Consortium at Scripps Institution of Oceanography for postdoctoral support. C.A. Rychert acknowledges funding from the Natural Environment Research Council (NE/M003507/1 and NE/K010654/1) and the European Research Council (GA638665). We would like to thank Yuguo Li, Ute Weckmann, and one anonymous

306 reviewer for their constructive comments which helped to improve the manuscript. Benjamin
307 Murphy is appreciated to give helpful comments too.

308

309 **References**

310 Agius, M.R., Harmon, N., Rychert, C.A., Tharimena, S. & Kendall, J.-M. (2018) Sediment
311 Characterization at the Equatorial Mid-Atlantic Ridge From P-to-S Teleseismic Phase
312 Conversions Recorded on the PI-LAB Experiment. *Geophys. Res. Lett.*, **45**, 12,244-
313 12,252. doi:10.1029/2018GL080565
314 Alekseev, D.A., Palshin, N.A. & Varentsov, I.M. (2009) Magnetotelluric dispersion relations in a
315 two-dimensional model of the coastal effect. *Izv., Phys. Solid Earth*, **45**, 167–170.
316 doi:10.1134/S1069351309020062
317 Bailey, R.C. (1977) Electromagnetic induction over the edge of a perfectly conducting ocean: the
318 H-polarization case. *Geophys. J. R. Astr. Soc.*, **48**, 385–392. doi:10.1111/j.1365-
319 246X.1977.tb03678.x
320 Boas, M.L. (2006) *Mathematical methods in the physical sciences*, Wiley.
321 Constable, S. & Cox, C.S. (1996) Marine controlled-source electromagnetic sounding: 2. The
322 PEGASUS experiment. *J. Geophys. Res. Solid Earth*, **101**, 5519–5530.
323 doi:10.1029/95JB03738
324 Constable, S. (2013) Review paper: Instrumentation for marine magnetotelluric and controlled
325 source electromagnetic sounding. *Geophys. Prospect.*, **61**, 505–532. doi:10.1111/j.1365-
326 2478.2012.01117.x

Constable, S., Key, K. & Lewis, L. (2009) Mapping offshore sedimentary structure using electromagnetic methods and terrain effects in marine magnetotelluric data. *Geophys. J. Int.*, **176**, 431–442. doi:10.1111/j.1365-246X.2008.03975.x

Cox, C. (1980) Electromagnetic induction in the oceans and inferences on the constitution of the earth. *Geophys. Surv.*, **4**, 137–156. doi:10.1007/BF01452963

Dosso, H.W. & Meng, Z.W. (1992) The coast effect response in geomagnetic field measurements. *Phys. Earth Planet. Inter.*, **70**, 39–56. doi:10.1016/0031-9201(92)90159-S

Harmon, N., Rychert, C., Agius, M., Tharimena, S., Bas, T.L., Kendall, J.M. & Constable, S. (2018) Marine Geophysical Investigation of the Chain Fracture Zone in the Equatorial Atlantic From the PI-LAB Experiment. *J. Geophys. Res. Solid Earth*, **123**, 11,016-11,030. doi:10.1029/2018JB015982

Heinson, G. & Constable, S. (1992) The electrical conductivity of the oceanic upper mantle. *Geophys. J. Int.*, **110**, 159–179. doi:10.1111/j.1365-246X.1992.tb00719.x

Heise, W. & Pous, J. (2003) Anomalous phases exceeding 90° in magnetotellurics: anisotropic model studies and a field example. *Geophys. J. Int.*, **155**, 308–318. doi:10.1046/j.1365-246X.2003.02050.x

Ichihara, H. & Mogi, T. (2009) A realistic 3-D resistivity model explaining anomalous large magnetotelluric phases: the L-shaped conductor model. *Geophys. J. Int.*, **179**, 14–17. doi:10.1111/j.1365-246X.2009.04310.x

Key, K. (2016) MARE2DEM: a 2-D inversion code for controlled-source electromagnetic and magnetotelluric data. *Geophys. J. Int.*, **207**, 571–588. doi:10.1093/gji/ggw290

348 Key, K. & Constable, S. (2011) Coast effect distortion of marine magnetotelluric data: Insights
349 from a pilot study offshore northeastern Japan. *Phys. Earth Planet. Inter.*, **184**, 194–207.
350 doi:10.1016/j.pepi.2010.11.008
351 Key, K., Constable, S., Liu, L. & Pommier, A. (2013) Electrical image of passive mantle
352 upwelling beneath the northern East Pacific Rise. *Nature*, **495**, 499–502.
353 doi:10.1038/nature11932
354 Lezaeta, P. & Haak, V. (2003) Beyond magnetotelluric decomposition: Induction, current
355 channeling, and magnetotelluric phases over 90°. *J. Geophys. Res. Solid Earth*, **108**.
356 doi:10.1029/2001JB000990
357 Mackie, R.L., Bennett, B.R. & Madden, T.R. (1988) Long-Period Magnetotelluric Measurements
358 Near the Central California Coast: A Land-Locked View of the Conductivity Structure
359 Under the Pacific Ocean. *Geophys. J.*, **95**, 181–194. doi:10.1111/j.1365-
360 246X.1988.tb00459.x
361 Menvielle, M., Rossignol, J.C. & Tarits, P. (1982) The coast effect in terms of deviated electric
362 currents: a numerical study. *Phys. Earth Planet. Inter.*, **28**, 118–128. doi:10.1016/0031-
363 9201(82)90077-2
364 Monteiro Santos, F.A., Nolasco, M., Almeida, E.P., Pous, J. & Mendes-Victor, L.A. (2001)
365 Coast effects on magnetic and magnetotelluric transfer functions and their correction:
366 application to MT soundings carried out in SW Iberia. *Earth and Planet. Sci. Lett.*, **186**,
367 283–295. doi:10.1016/S0012-821X(01)00237-0
368 Naif, S., Key, K., Constable, S. & Evans, R.L. (2013) Melt-rich channel observed at the
369 lithosphere–asthenosphere boundary. *Nature*, **495**, 356–359. doi:10.1038/nature11939

370 Nolasco, R., Tarits, P., Filloux, J.H. & Chave, A.D. (1998) Magnetotelluric imaging of the
371 Society Islands hotspot. *J. Geophys. Res.*, **103**, 30287–30309. doi:10.1029/98JB02129
372 Parkinson, W.D. & Jones, F.W. (1979) The geomagnetic coast effect. *Rev. Geophys.*, **17**, 1999–
373 2015. doi:10.1029/RG017i008p01999
374 Pedersen, L.B. & Engels, M. (2005) Routine 2D inversion of magnetotelluric data using the
375 determinant of the impedance tensor. *Geophysics*, **70**, G33–G41. doi:10.1190/1.1897032
376 Pek, J. & Verner, T. (1997) Finite-difference modelling of magnetotelluric fields in two-
377 dimensional anisotropic media. *Geophys. J. Int.*, **128**, 505–521. doi:10.1111/j.1365-
378 246X.1997.tb05314.x
379 Price, A.T. (1949) The induction of electric currents in non-uniform thin sheets and shells. *Q. J.*
380 *Mechanics Appl. Math.*, **2**, 283–310. doi:10.1093/qjmam/2.3.283
381 Ranganayaki, R.P. & Madden, T.R. (1980) Generalized thin sheet analysis in magnetotellurics:
382 an extension of Price's analysis. *Geophys. J. Int.*, **60**, 445–457. doi:10.1111/j.1365-
383 246X.1980.tb04820.x
384 Raziman, T.V. & Martin, O.J.F. (2016) Does the real part contain all the physical information? *J.*
385 *Optics*, **18**, 095002. doi:10.1088/2040-8978/18/9/095002
386 Selway, K., Thiel, S. & Key, K. (2012) A simple 2-D explanation for negative phases in TE
387 magnetotelluric data. *Geophys. J. Int.*, **188**, 945–958. doi:10.1111/j.1365-
388 246X.2011.05312.x
389 Stratton, J.A. (2015) Stress and Energy. in *Electromagnetic Theory*, pp. 83–159, Wiley-
390 Blackwell. doi:10.1002/9781119134640.ch2
391 Weckmann, U., Ritter, O. & Haak, V. (2003) A magnetotelluric study of the Damara Belt in
392 Namibia: 2. MT phases over 90° reveal the internal structure of the Waterberg

393 Fault/Omaruru Lineament. *Phys. Earth Planet. Inter.*, **138**, 91–112. doi:10.1016/S0031-
394 9201(03)00079-7
395 Worzewski, T., Jegen, M., Kopp, H., Brasse, H. & Castillo, W.T. (2011) Magnetotelluric image
396 of the fluid cycle in the Costa Rican subduction zone. *Nature Geosci.*, **4**, 108–111.
397 doi:10.1038/ngeo1041
398 Worzewski, T., Jegen, M. & Swidinsky, A. (2012) Approximations for the 2-D coast effect on
399 marine magnetotelluric data. *Geophys. J. Int.*, **189**, 357–368. doi:10.1111/j.1365-
400 246X.2012.05385.x
401
402

403 **Figures**

404 Figure 1

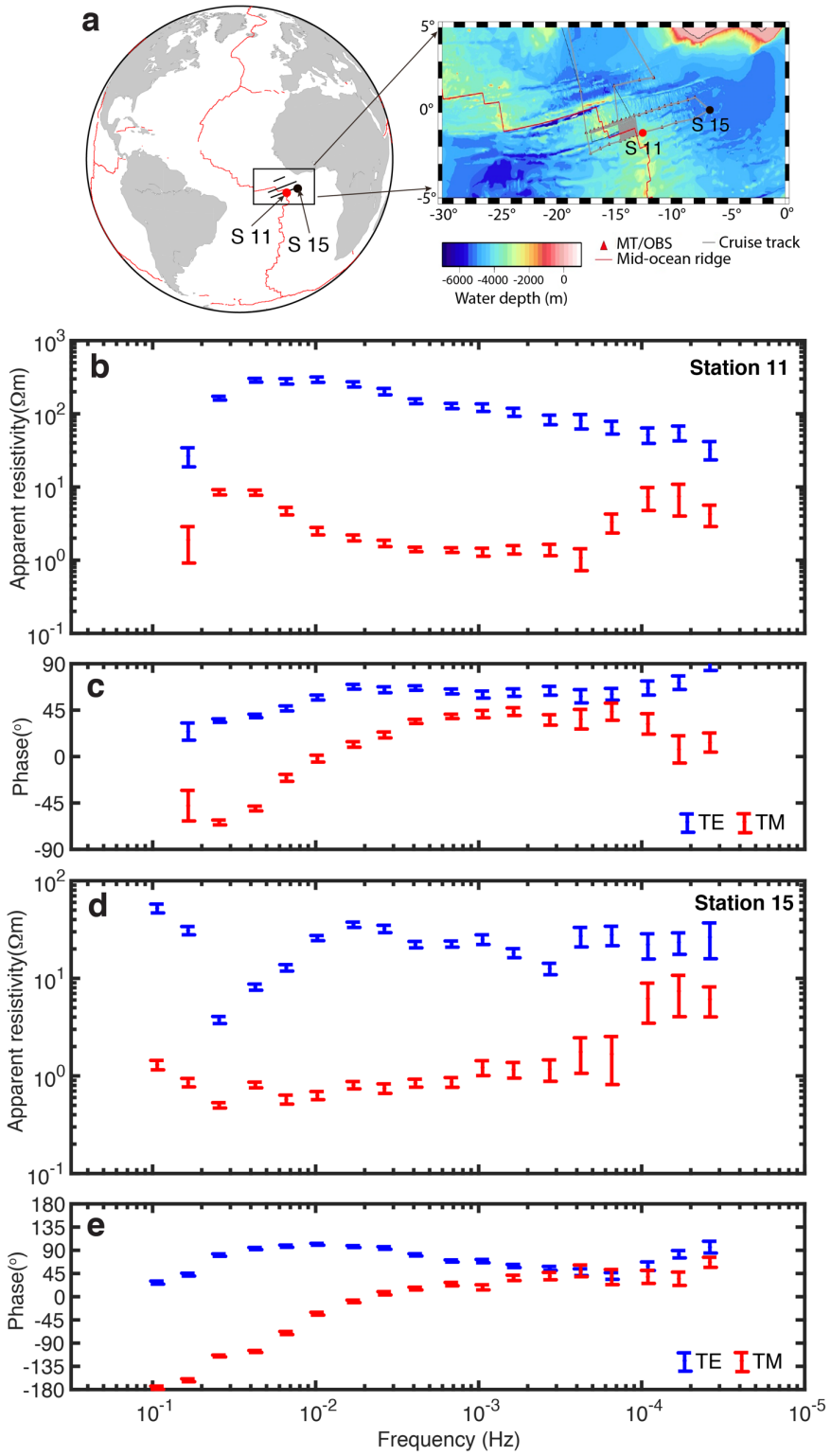

405

406 **Figure 1.** The research area at MAR (inset) and examples of distorted MT data. (a) Research area.
407 (b) Apparent resistivity and (c) phase data at station 11 near the MAR. (d) Apparent resistivity and
408 (e) phase data at station 15 closer to the African coast. Blue and red colors mark TE and TM-mode
409 data, respectively. TM-mode negative phases exist from station 11 to station 15 at the eastern side
410 of the profile.
411

412 Figure 2

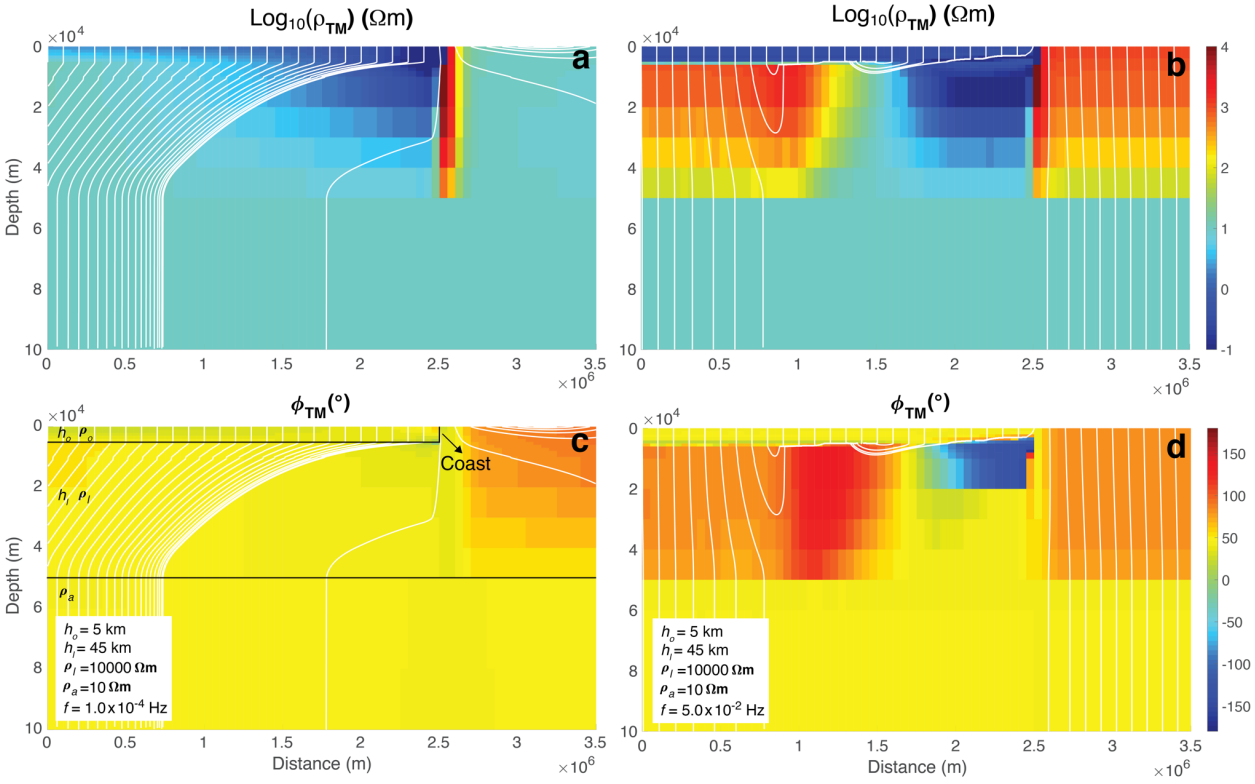

413

414 **Figure 2.** Comparison of TM-mode apparent resistivities and phases at two frequencies. TM-mode
415 apparent resistivities, (a) and (b), and TM-mode phases, (c) and (d), at frequencies of 1.0×10^{-4} and
416 5.0×10^{-2} Hz, respectively. Black lines in (c) represent the boundaries of the model used. h_o and ρ_o
417 represent the depth and resistivity of the ocean. h_l and ρ_l represent the thickness and resistivity of
418 the seafloor/lithosphere, and ρ_a represents the resistivity of conductive/asthenospheric layer. ρ_o is
419 fixed as 0.33 Ωm in the study. White streamlines represent the Poynting vector direction, showing
420 EM energy propagation. The turning of the Poynting vector from the coast to the ocean
421 corresponds to the negative phases of TM-mode data. TM-mode coast effect is, however,
422 frequency-dependent.

423

424 Figure 3

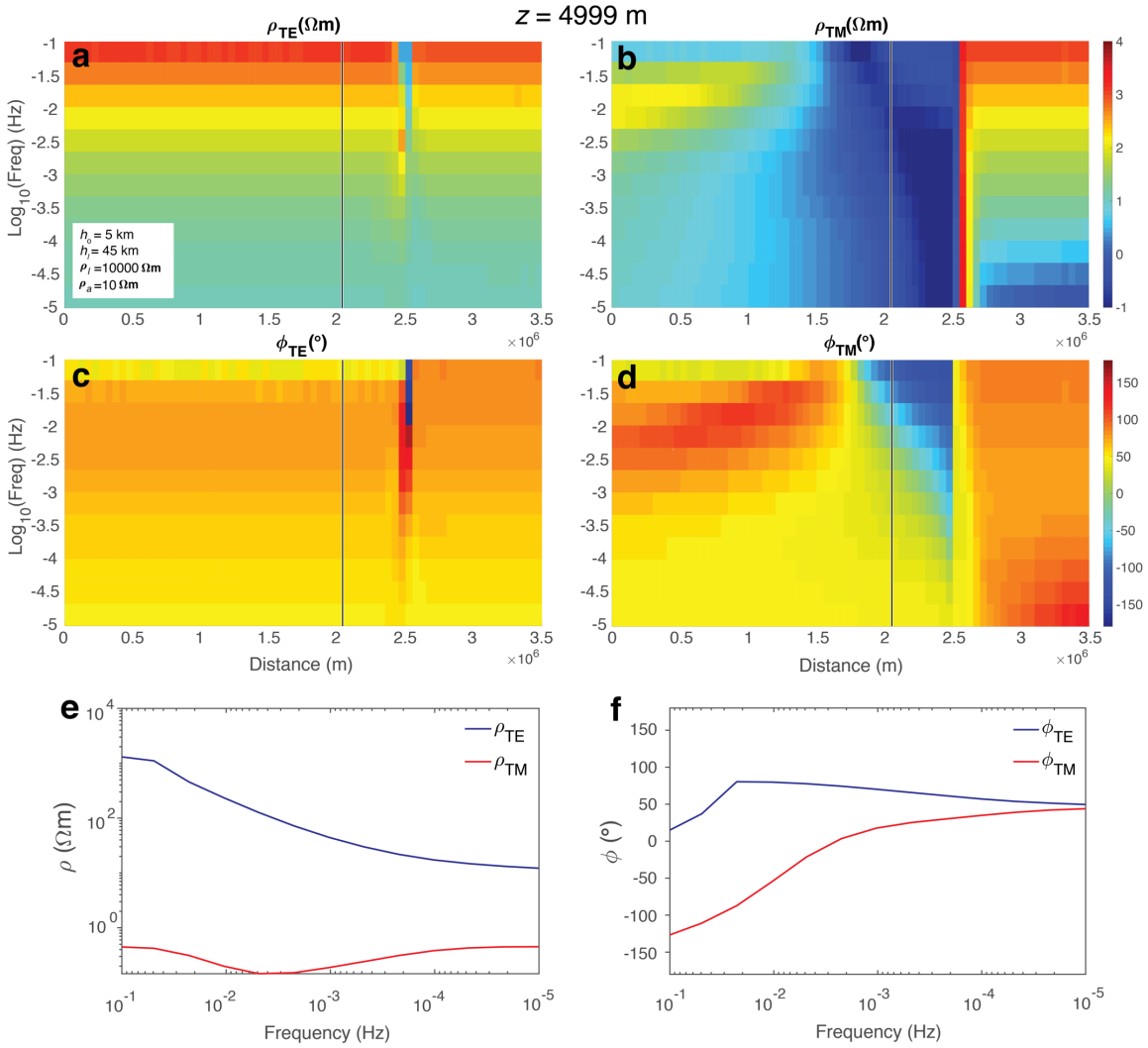

425

426 **Figure 3**. TE and TM-mode apparent resistivities, (a) and (b), and phases, (c) and (d), at one meter
427 above seafloor based on the model in Fig. 2. (e) and (f) apparent resistivities and phases selected
428 along the frequency axis at a 2050 km distance (marked as black lines in a-d). Thirteen frequencies
429 were used from 1.0×10^{-5} to 0.1 Hz. TM-mode coast effect shows frequency-dependence, which
430 indicates induction phenomenon.

431

Figure 4

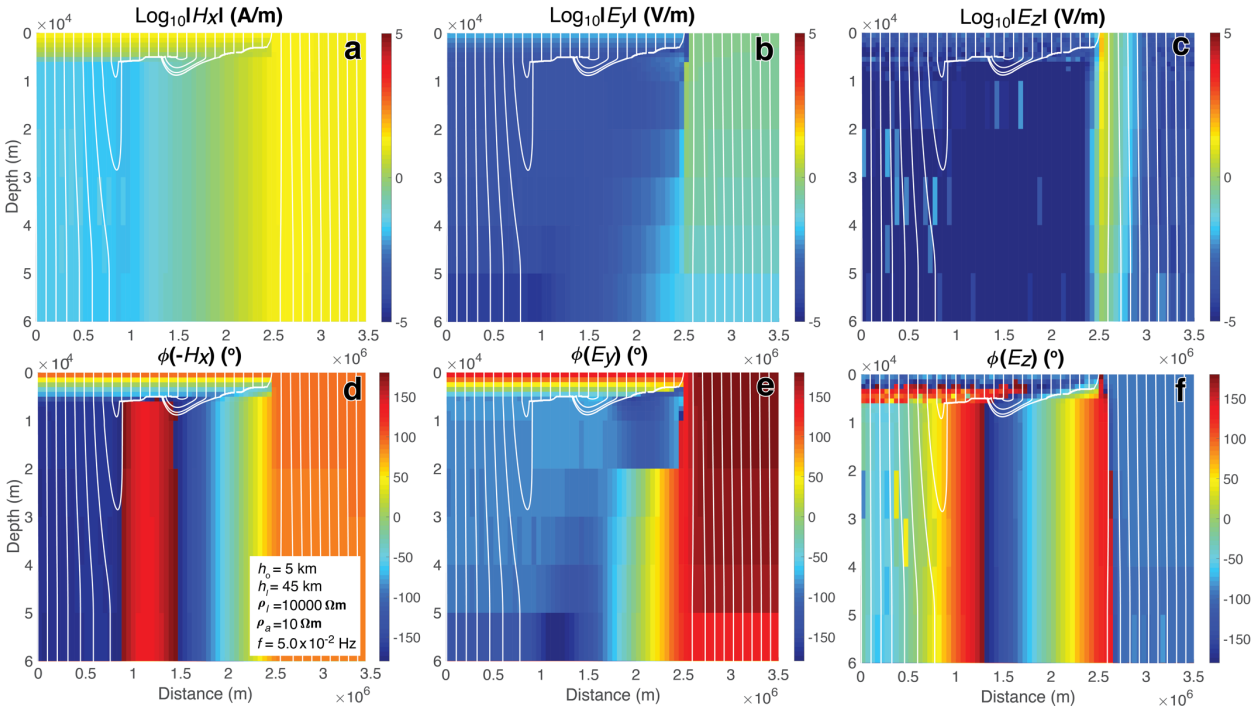

Figure 4. Amplitudes of (a) H_x, (b) E_y, and (c) E_z fields, and phases of (d) - H_x, (e) E_y, and (f) E_z fields. White streamlines represent the Poynting vector. When H_x changes directions, for example at distances of 1000 to 1500 km and 1800 to 2500 km, the Poynting vector changes propagation direction. E_z field has small values, thus it has slight influence of inaccuracy.

440 Figure 5

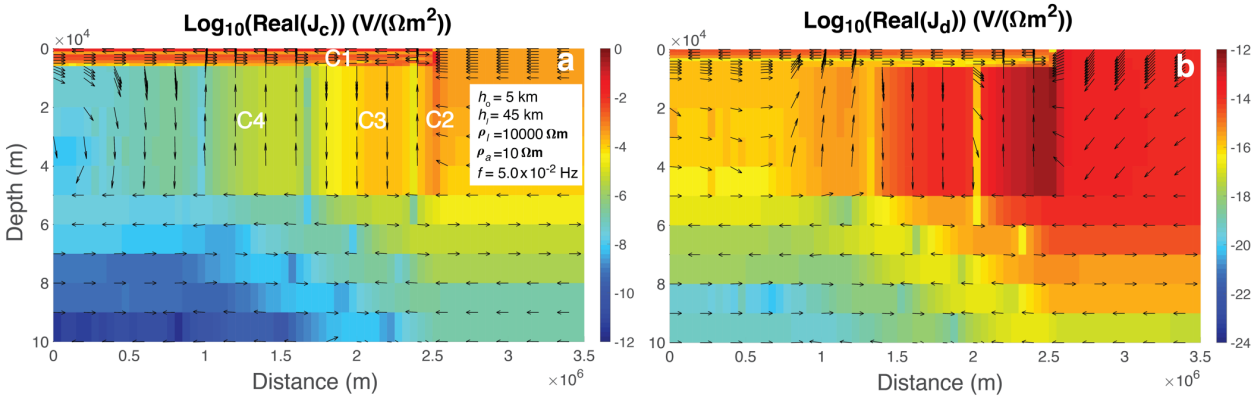

441

442 **Figure 5.** The real components of the conduction and displacement current density (Equation 6),
443 (a) and (b), respectively. The arrows only represent flowing directions of the currents. The reason
444 of using real component is that it represents the physical quantities. Displacement current is
445 negligible compared to conduction current, so that this term is dropped in later usage.

446

447

448 Figure 6

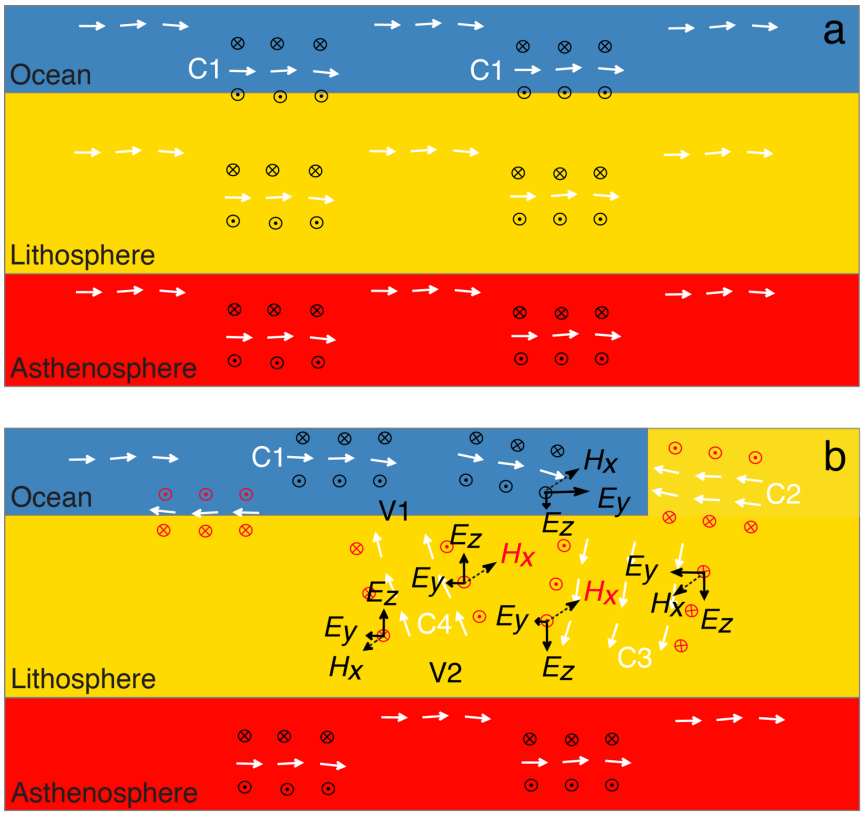

449

450 **Figure 6.** The sketch of current flows. (a) current flows without a coast, and (b) current flows with
451 a coast. Current flows are represented by the white arrows. Four types of currents are shown in
452 (b), marked as C1, C2, C3, and C4. The corresponding magnetic fields are marked with circles
453 based on right-hand rule. EM fields are shown at the coast area. All currents flow in the same
454 direction when the coast is not existed. Thus, phase reversal cannot be caused by a layered model.
455 The currents, however, change flowing directions due to the influence of the coast, especially in
456 the lithosphere.

457

458 Figure 7

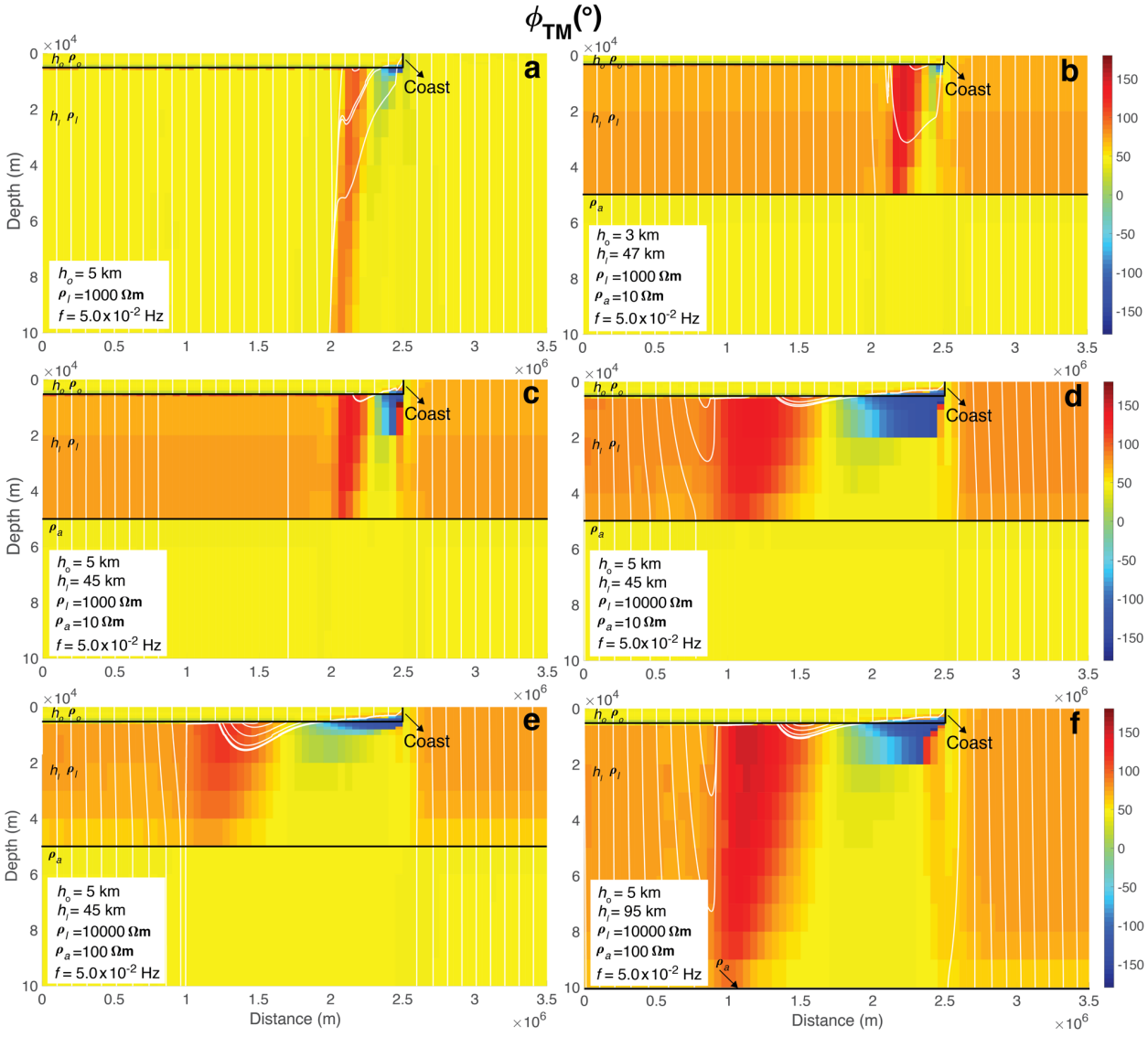

459

460 **Figure 7.** TM-mode phases for various models with one conductive layer beneath the
461 seafloor/lithosphere, except for (a). All the parameters have the same physical meaning as in Fig.
462 2. The coast position and the resistivity of ocean are same as in Fig. 2. Black lines mark the
463 boundaries in the models. The upward propagation of the Poynting vectors, white streamlines, is

464 directly related to negative phases. The negative phases are sensitive to the LAB and also other
465 parameters of the models.
466

467 Figure 8

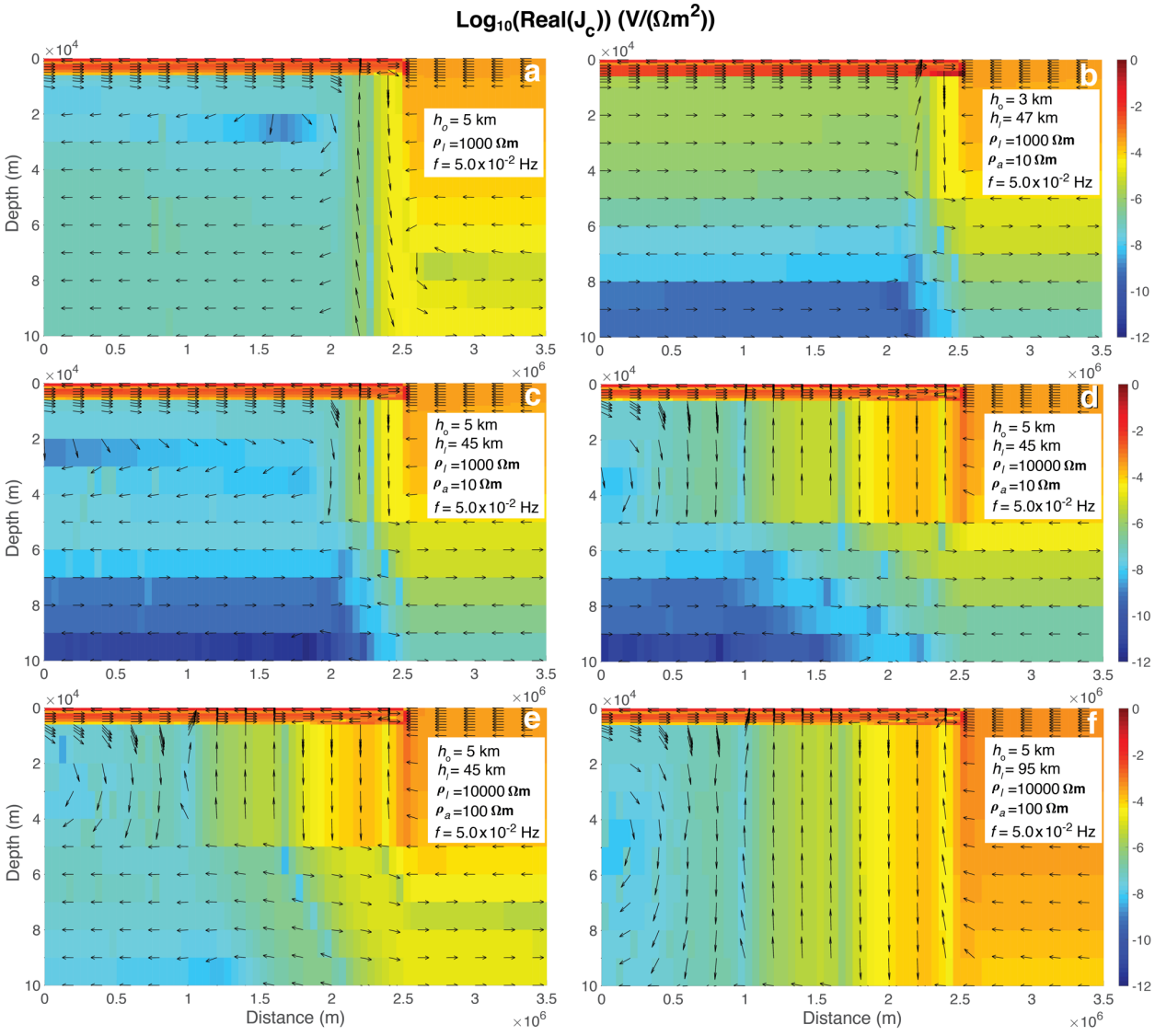

468

469 **Figure 8.** Real part of conduction current density based on the same models in Fig. 7. The arrows

470 represent the direction of current flows as Fig. 5. The low current density under the seafloor are

471 related to the changes of current directions.

472